Assessing Groundwater Impacts of Geothermal Development through Integrated Modeling: Insights from Ulumbu with Broader Applications

Angela Benedicta Horta, John O'Sullivan, and Michael Gravatt

Geothermal Institute, University of Auckland, 70 Symonds Street, Grafton, Auckland 1010, New Zealand

ahor443@aucklanduni.ac.nz

Keywords: *Geothermal, Modelling, Groundwater, Agriculture.*

ABSTRACT

Social issues such as agricultural disruption, water scarcity, health risks, and natural disasters remain key challenges in geothermal energy development in Indonesia, often delaying project implementation and reducing public acceptance. This study investigates the impact of geothermal production at the Ulumbu Geothermal Field on the local water table and its potential implications for nearby agricultural areas.

A three-dimensional conceptual model was constructed using Leapfrog™, incorporating geological, structural, and alteration data. This model was then translated into a numerical reservoir model using AUTOUGH2. Refinements were applied to the shallow subsurface to ensure simulation stability and accurately capture water table responses.

Two calibration phases were performed. The first involved natural-state calibration by adjusting permeability values and introducing a hot plate to simulate subsurface heat input. This confirmed that Ulumbu is a vapor-dominated system with reservoir temperatures ranging from 220–240°C. The second phase matched production history by refining porosity and relative permeability to reproduce the enthalpy and mass flow of well ULB-02, which produced dry steam with enthalpy values between 2803 and 2787 kJ/kg from 2012 to 2025.

After calibration, pressure changes in blocks associated with agricultural zones were evaluated and converted into water table variations. Results indicate a maximum water table decline of only 4.6 mm, considered negligible and unlikely to impact agricultural sustainability. This study provides a robust modelling framework for assessing the groundwater impacts of geothermal production and contributes to addressing critical social concerns associated with geothermal development in Indonesia.

1. INTRODUCTION

Indonesia has the second-largest geothermal potential in the world, with a total capacity of 29,000 MWe. Flores Island contributes to this with a potential of 959.5 MWe. However, this potential has not been fully utilised, as only 20.5 MWe of the total 959.5 MWe has been developed, specifically in the Ulumbu, Mataloko, and Sokoria fields.

The Ulumbu Field is located in Manggarai Regency, 13 km from Ruteng, East Nusa Tenggara. The geothermal system at Ulumbu Field is vapor-dominated, underlying a liquid-dominated system, with temperatures ranging from 230-240°C (Kurniawan et al. 2019). According to the Ministry of Energy and Mineral Resources Regulation No. 40 of 2014 and the 35 GW program discussion meeting, the Ulumbu Geothermal Power Plant (PLTP) is targeted to produce 20 MWe of electricity. However, since it started operating in 2011, Ulumbu Field has only been able to deliver at a capacity of 4×2.5 MWe, and production has continued to decline, leading to an operational adjustment in November 2018 to 3×2.5 MWe. (Hilah and Subekti, Dipl. Eng., M.E. 2022). PLN, the company operating Ulumbu Field, has planned to add units 5 and 6 to increase production at the field, but to this day, there has been significant resistance from the community.

The community has voiced various concerns, one of which is a decline in agricultural yields, such as cloves, which, before the Ulumbu geothermal field began operations, reached 120 kg per year, but then drastically decreased to 50 kg per year after the field started producing (Teredi, Sukarno, and Jaya 2022). This decline in production is suggested to be associated with a decrease in the water table. One cause of change in the water table could be production from the geothermal field. Competition between the water required for community use and the water used in the geothermal industry is of concern. However, other factors can impact the crops, such as quantity and seasonality of rainfall, soil properties, crop and pasture species, management options, land type, groundwater depth, and quality.

Because of the possibility of many factors that can impact the crops, this paper aims to investigate the connection between the utilisation of geothermal energy as a source of electricity and the decrease in the water table around the Ulumbu Field. This research is expected not only to provide insights into effective development scenarios for the Ulumbu Field, considering both economic and environmental aspects, so that neither the company nor the community is harmed, but also to provide insight for other cases that have the same concern on the water table, like in Rotorua, New Zealand.

2. METHODOLOGY

2.1 3D Model Construction

The 3D model construction process begins with importing all surface and subsurface data into Leapfrog Software. This step is crucial, as the model's accuracy depends on the quality and completeness of the imported data; the less data included, the greater the uncertainty in the model. This is followed by various setup procedures, which will be discussed below. Figure 1 illustrates the workflow for creating the 3D model.

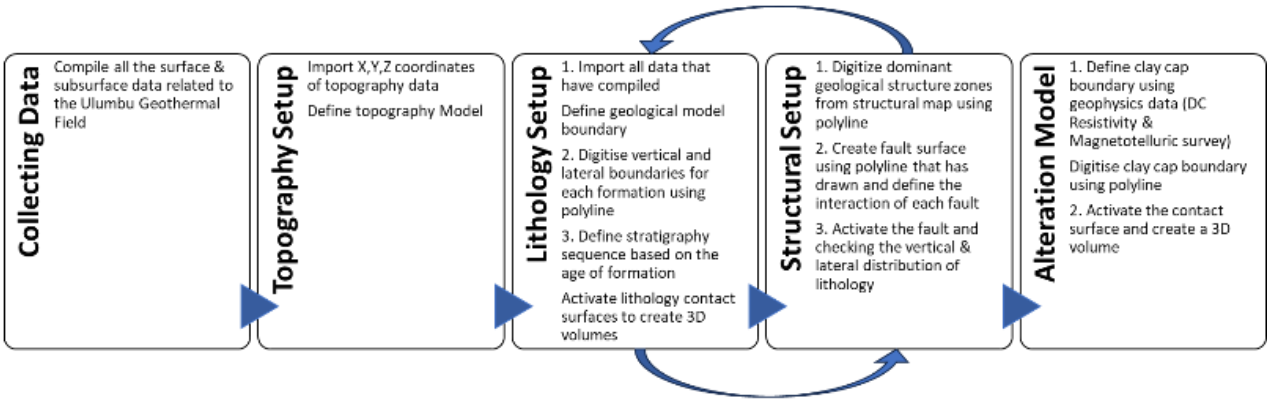

Figure 1: Workflow for building the 3D models of Ulumbu Geothermal Field.

2.1.1 Topography Setup

Leapfrog has a Topography folder where a surface representing the topography is generated. This topography automatically serves as the upper boundary of the model, eliminating the "air" volume. The area of topography imported into Leapfrog covers about 50 km² × 50 km² around the Ulumbu fumarole. This extensive area was chosen to capture the whole geothermal system around Ulumbu, ensuring a comprehensive representation of the geothermal dynamics.

2.1.2 Lithology Setup

The process of setting up the lithology begins with defining the area of the model, which is a 40 km² by 40 km² region. This area encompasses all the surface manifestations found in the Ulumbu field. The next step is selecting the lithology to be used in Leapfrog, which, in this case, will be based on the local geological map presented in Figure 2. From the horizontal view of the map, there are over twenty different rock types. Volcanic and sedimentary rocks are categorised based on the eruption sources from various mountains.

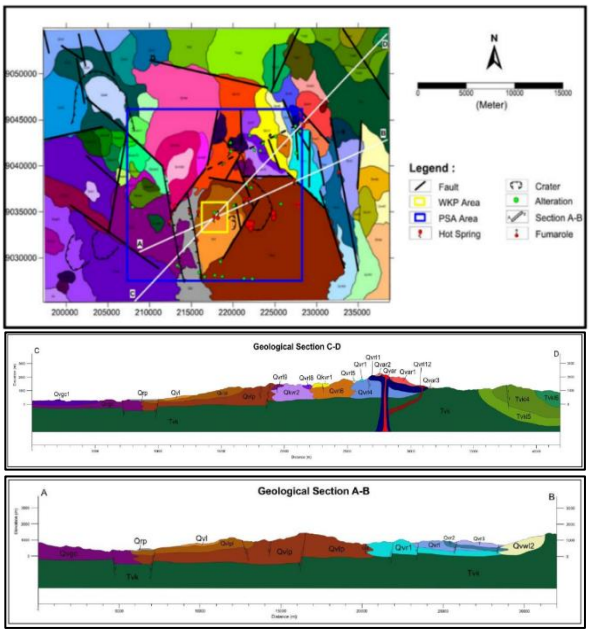

Figure 2: Volcanostratigraphy Map. (Modified from EBTKE 2016)

For simplicity, this study focuses on three main mountain complexes. (Yuono and Daud 2020): Mt. Golo Curububeng, which is close to Mt. Mandasawu; Mt. Likong, where the existing wells are located; and Mt. Ranakah. Once the lithology for the geological model is defined, surface contacts between each lithology must be created. These contacts will provide the volume of each lithology once activated.

Table 1: Overview of the stratigraphy rock units in Ulumbu Geothermal Field (Modified from Widiatmoro and Nusiaputra 2020; Yuono and Daud 2020; EBTKE 2016)

Rock Unit	Abbreviation	Geologic Age	
		Period	Epoch
Pyroclastic Material	Qrp	Quatenary	Holocene
Pyroclastic & Lava, Volcanic Unit of Mt. Likong	QVU	Quatenary	Pleistocene
Pyroclastic & Lava, Volcanic Unit of Mt. Likong	QVM	Quatenary	Pleistocene
Dominantly Pyroclastic, Volcanic Unit of Mt. Likong	QVL	Quatenary	Pleistocene
Dominantly Pyroclastic, Volcanic Product of Mt. Ranakah	Qvr1	Quatenary	Pleistocene
Dominantly Pyroclastic, Volcanic Unit of Mt. Golo Curunumbeng	Qvgc	Quatenary	Pleistocene
Sediment, Lava, Pyroclastic, Material of Mt. Kiro	Tvk	Tertiary	Pliocene to Late Miocene

Table 1 provides an overview of the stratigraphic sequence of rock units, which serves as the order for the contact surfaces when forming the model. As shown in Table 1, the material from Mt. Golo Curunumbeng forms the oldest rock unit. This is supported by the analysis of (Yuono and Daud 2020), which indicates that the magma movement direction was from the Northeast to the Southwest, originating from Mt. Golo Curunumbeng, followed by Mt. Ranakah and Mt. Likong. Figure 4 compares the vertical and horizontal lithology distribution between the newly developed digital conceptual model and that from the local geological maps. A strong correlation is observed between the two maps. However, the geological map developed in this study extends further south, where the lithological distribution aligns with the regional geological map shown in Figure 3. Therefore, in Figure 4, the updated geological map appears slightly larger in the southern direction.

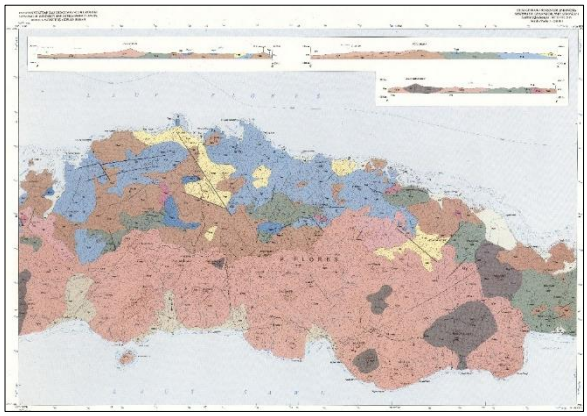

Figure 3: Regional Geological Map of the Ruteng Quadrangle, East Nusa Tenggara. (Modified from Geological Research and Development Center)

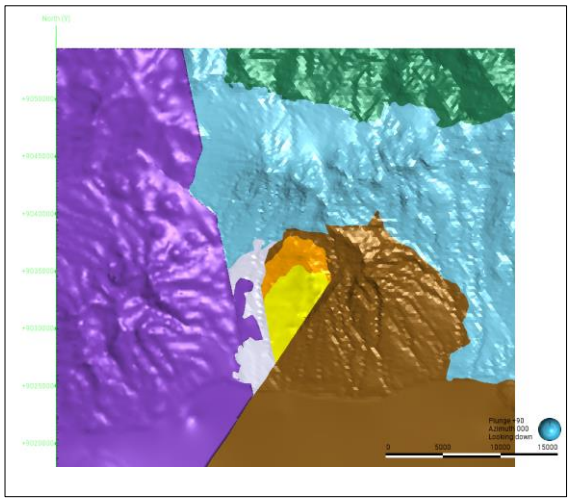

Figure 4: Lithological Configuration of the Ulumbu Geothermal Field from the newly developed digital conceptual model (Modified from EBTKE 2016)

2.1.3 Structural Setup

The structural setup involves incorporating faults into the geological model designed to control fluid flow in the Ulumbu Geothermal system. Only the main faults were digitised and included in the model for this study. According to (EBTKE 2016; Kurniawan et al. 2019)The primary fault directions are NE-SW, NNW-SSE, NW-SE, and ESE-WNW. However, not all faults in these directions are included in the model. Surface manifestations are another key factor in selecting which faults to incorporate into the Leapfrog model. The presence or absence of surface manifestations around a fault helps determine whether the fault is acting as a conduit or a barrier.

Figure 5 illustrates the faults used in the model. The faults that act as conduits are NNW-SSE and NE-SW, as surface manifestations are observed around these faults. The caldera is expected to function as a barrier based on the different surface manifestations examined. To the west of the caldera, sulphate hot spring waters are found, such as at Wae Wera and Wae Enggal, while to the east, carbonate hot springs are located, such as at Rondorowing. This suggests the caldera does not create a permeable pathway for fluids to surface in the exact location. Additionally, the carbonate hot spring at Rondorowing is found near the NW-SE fault, reinforcing the idea that the NW-SE fault serves as a fluid pathway, while the caldera does not.

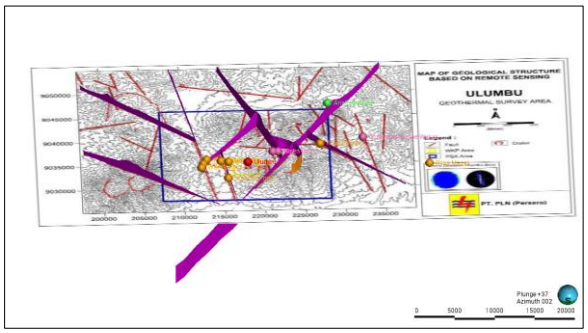

Figure 5: The fault structures in the Ulumbu Geothermal Field, along with surface manifestations, are illustrated as circular symbols overlaid on the Local Structural Map

2.1.4 Alteration Model

This model incorporates the clay cap as a top barrier for fluid flow. The clay cap is a low-permeability rock that forms through alteration processes. This study defines the clay cap using geophysical methods, specifically DC resistivity and magneto telluric surveys. Additionally, surface manifestations offer further insights into the lateral extension of the clay cap. As a result, the updoming is located beneath the Ulumbu fumarole, causing the clay cap to be significantly thinner in this region and thicker at the edges of the clay cap model. The thickness of the clay cap in this model ranges from 400 to 800 m, which aligns with data from (Sulasdi 1996).

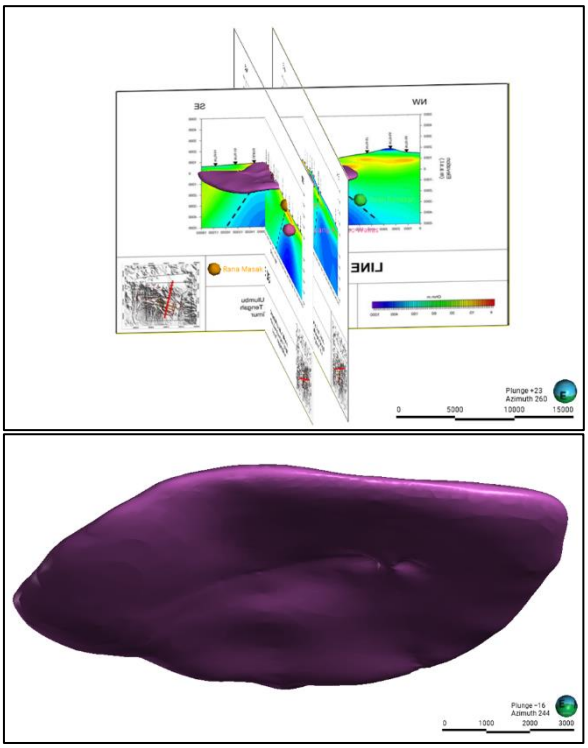

Figure 6: Clay Cap Zone (purple volume) delineated from magneto telluric data, along with the distribution of surface manifestation (coloured circular shapes)

2.2 Numerical Model

Numerical simulation is the next step after developing a conceptual model. It transforms the qualitative insights of the conceptual model into a quantitative framework by applying discretisation techniques (e.g., grids or meshes) and governing physical equations (such as mass and energy conservation laws). The numerical model simulates key reservoir behaviour, including the pressure and temperature distribution, production and reinjection performance, and long-term reservoir sustainability.

2.2.1 Tough2 Model Generation

In the Ulumbu numerical model, the grid spans an area of 21,000 m × 19,000 m and comprises approximately 65,583 blocks, the largest of which measure 800 m × 800 m. The vertical thickness of these blocks varies from 850 m at depth to 100 m near the surface. The block size is reduced to 400 × 400 m to improve accuracy in key zones, enhancing resolution in areas with significant fluid flow. This level of detail is essential for capturing complex interactions within the geothermal reservoir, particularly in boiling zones. Additional refinement is applied to shallow regions to support stable, accurate simulations responding to water table fluctuations. This ensures the model remains robust under varying groundwater conditions. Figure 7 illustrates the model setup, including fault overlays.

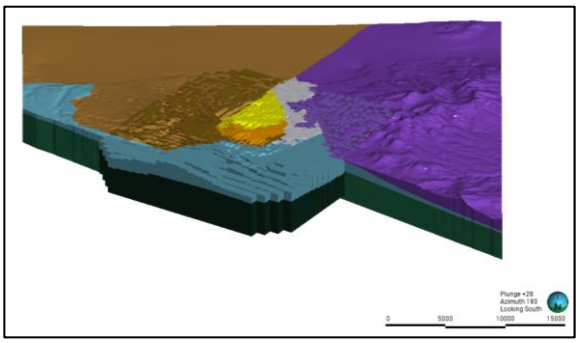

Figure 7: The Leapfrog model (right) and the corresponding generated TOUGH2 model (left), with grid symbol

2.2.2 Rock Type Mapping & Properties

In this study, the original seven rock types used in the conceptual model were expanded into 230 distinct rock types (shown in Appendix A) in the numerical model. For example, the TVK rock unit, which serves as the basement in the 3D conceptual model, is divided into numerical rock types such as B0021, BE021, B0010, and BAE21. This naming convention aligns with geological structures and alteration zones and allows for detailed characterisation in the simulation. Table 2 provides definitions and descriptions for each rock type name.

After the naming convention is established, the next step involves assigning the physical properties required for reservoir simulation, including density, porosity, permeability, thermal conductivity, and specific heat capacity. This process is carried out using PyTOUGH scripts. However, TIM also allows users to add new rock types, assign new properties, or modify existing ones as needed. Figure 8 shows the top distribution of the rock properties for the Ulumbu Geothermal Field.

Table 2: Example of the Rock Type Naming Convection

Formation: Basement	1st fault intersected	2nd fault intersected	Zone	Size	Meaning
B	0	0	2	1	Rock-type Basement inside the reservoir with medium block
B	E	0	2	1	Rock-type Basement intersected with fault E inside the reservoir with a medium block
B	0	0	1	0	Rock-type Basement outside the reservoir with outer block
B	A	E	2	1	Rock-type Basement intersect with both fault A & E inside the reservoir with a medium block.

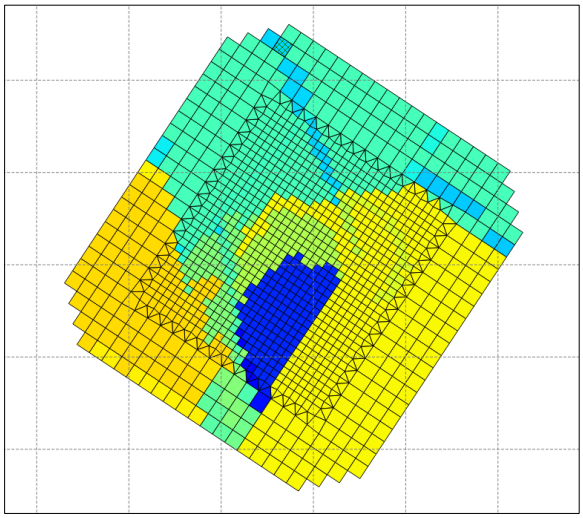

Figure 8: The top-view of the distribution of rock properties for the Ulumbu Geothermal Field

2.2.3 Boundary Condition

Setting appropriate boundary conditions in a numerical simulation is a crucial aspect of geothermal modelling, as it determines how the geothermal system interacts with its surrounding environment. Essentially, boundary conditions define the rules for what can enter or exit the reservoir model. According to (M. O'Sullivan and J. O'Sullivan 2016) and (J. O'Sullivan et al. 2023) There are three main boundary types based on their physical location in the model: top, side, and bottom boundaries.

The top boundary condition in this model is defined as a "dry" atmospheric interface (J. O'Sullivan et al. 2023), with pressure fixed at atmospheric levels (~1 bara) and temperature set to the area's mean annual surface temperature of 26°C. The EOS3 module was employed to define the thermophysical properties of water and air, essential for solving mass and energy balance equations (Pruess, Oldenburg, and Moridis 1999). Hydrological input from precipitation was incorporated into the model using an annual rainfall distribution that varies by block, with an average of 2,362.5 mm/year. An infiltration rate of 10% was assumed to represent recharge from meteoric water. This assumption is consistent with the findings of the study of (Kurniawan et al. 2019). The uppermost layer is assigned high permeability to simulate effective percolation and facilitate downward infiltration into the subsurface system.

No-flow boundary conditions are applied for the side boundary, indicating that neither heat nor mass can enter or leave the system. To avoid boundary-related artifacts, the

side boundaries are positioned at a sufficient distance, approximately 4 to 5 km beyond the resistivity-defined extent of the geothermal system (Nugraha et al. 2022).

Moreover, for the bottom boundary, a hot plate bottom boundary condition is applied, reflecting the characteristics of a vapor-dominated geothermal system (M. O'Sullivan and J. O'Sullivan 2016). This boundary assumes a constant high temperature and saturated vapor conditions at the model's base, set at 320°C and a gas saturation of 0.5, respectively, to achieve a pressure and temperature that align with measured data. A mass flux boundary condition would typically generate a relatively wet two-phase zone, preventing the production of dry steam from wells. Therefore, it is not suitable for this particular case.

2.3 Model Calibration

The objective of model calibration is to ensure that the simulation results closely align with observed field data. This process is typically divided into two main stages. The first stage, referred to as natural state calibration, involves adjusting the model to reproduce the observed pressure and temperature distributions under pre-exploitation conditions, where the reservoir is assumed to be in a steady state and no wells have been drilled. The second stage, known as history matching, is conducted once wells have been drilled and production has commenced. This phase focuses on matching the model to observed production data, such as mass flow rates and enthalpy.

2.3.1 Calibrated Natural State Model

In the natural state simulation, the primary parameters adjusted to match the observed pressure and temperature data from wells in the Ulumbu field are the rock permeability and the hot plate boundary condition**,** including its temperature and vapor saturation. In contrast, for liquid-dominated systems, where the bottom boundary is typically represented by hot water recharge, both the mass input and its spatial distribution can be tuned to achieve a good match.

For the Ulumbu Geothermal Field, three wells were used in the natural state calibration: ULB-01, ULB-02, and ULB-03. ULB-01 is the deepest and most informative**,** providing a more comprehensive set of pressure and temperature data (as shown in Figure 9). The presence of nearly constant pressure between depths of -250 to -375 m, accompanied by a nearly constant temperature, indicates that the Ulumbu field is vapor-dominated. This observation aligns with the theoretical framework described by (Grant and Bixley 2011), which characterises vapor-dominated reservoirs as containing steam with pressures close to steam static and temperatures near the saturation point.

Another critical factor adjusted during calibration was the temperature and spatial extent of the steam zone at the hot plate. If the steam-saturated area is too large, steam may expand into deeper zones that should remain liquid, distorting the model. Conversely, if the steam input is too small, the resulting pressure and temperature will be insufficient, leading to poor calibration results. Therefore, achieving a balance between rock permeability distribution and the parameters of the hot plate is essential for accurately representing the reservoir's natural state.

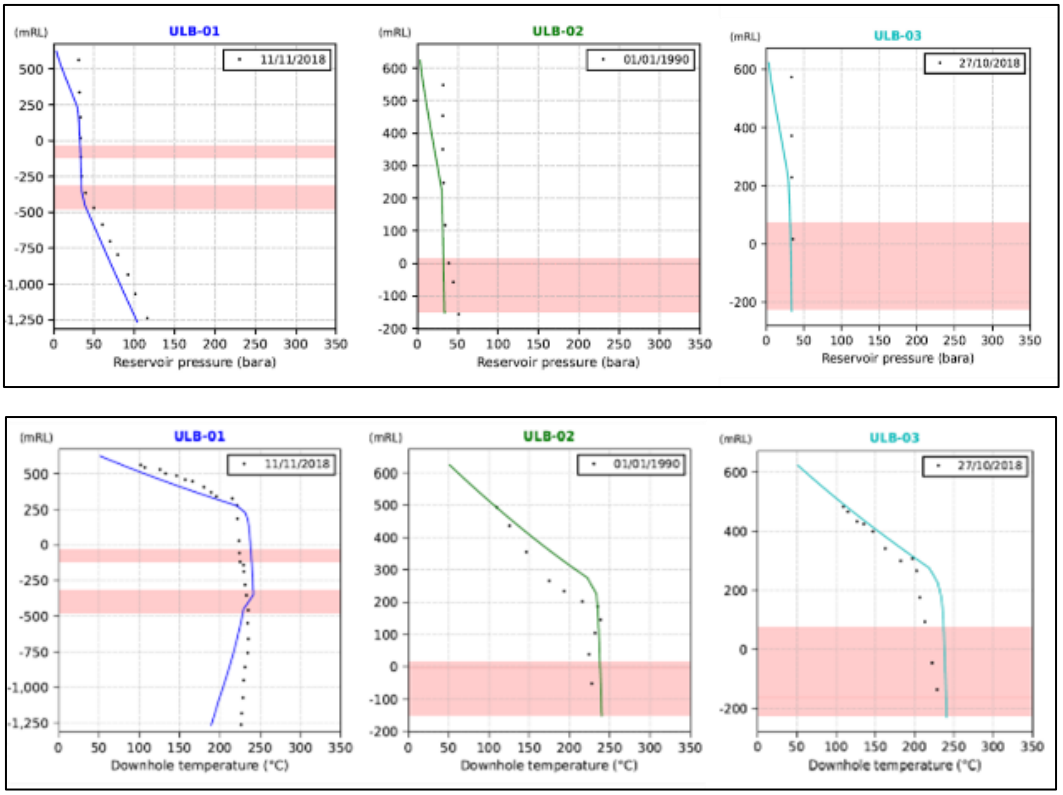

Figure 9: Matching Pressure and Temperature Well Profiles in the Ulumbu Geothermal Field

ISSN 2703-4275

The natural state calibration results are presented in Figure 9 and show a successful match with the measured temperature data from the three wells. However, at ULB-01 below -500 m depth, the simulated temperature is lower than the measured values. In this case, the measured data at that depth is considered unreliable due to the presence of a convective steam zone above -500 m, which likely caused artificially elevated temperature readings. Based on this natural state analysis, the primary driving mechanism for changes in reservoir pressure and temperature is boiling, rather than liquid pressure, due to the presence of steam. This finding further supports the classification of the Ulumbu Geothermal Field as a vapor-dominated system. Steam is observed to originate near the bottom of the well in a small area and expand upward as pressure decreases, eventually spreading laterally at specific depths due to high lateral permeability, as illustrated in Figure 10

The natural state result also aligns with the surface manifestations represented in the conceptual model. The bicarbonate hot spring located in the southwest (SW) is interpreted as an outflow zone, while the sulphate hot spring, situated beneath a fault, indicates an upflow zone (Figure 10). In this calibrated model, the water level is another critical parameter that must match the observed data. As shown in Figure 10, the modelled water level is approximately -350 m, which is consistent with the measured data presented in Figure 9.

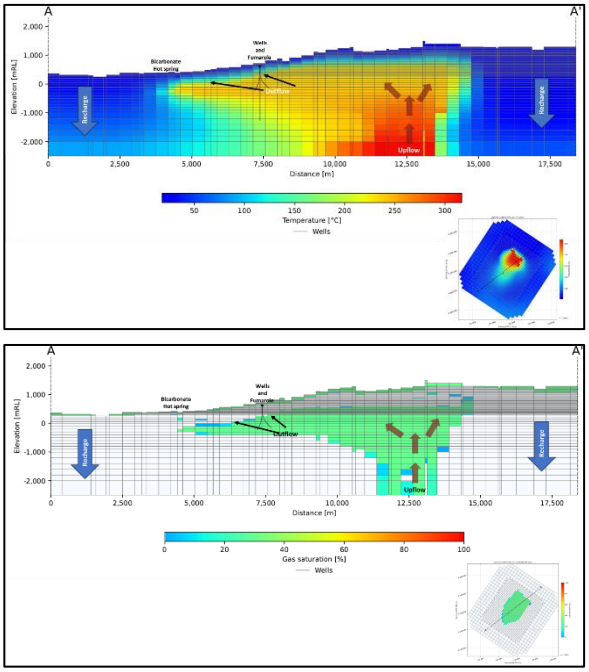

Figure 10: Temperature and gas distribution in the natural state model of the Ulumbu Geothermal Field

2.3.2 History Matching

After completing the natural state modelling, the next step is to perform history matching, which involves calibrating the model based on data collected during the production period of the wells. Model parameters must be adjusted to match observed and simulated data well. These changes can also affect the natural state model, necessitating a re-run to ensure consistency and that the natural state match has not been degraded. Additional iterations are often required to obtain an acceptable fit for the natural state and the production history. Due to data limitations in this study, only mass flow and enthalpy were used in the history matching process. Of the three wells drilled in Ulumbu since 2012, only ULB-02 has remained in continuous production. As a result, only ULB-02 was selected for production calibration. The available mass flow and enthalpy data were sourced from different references, resulting in data gaps. Mass flow data were obtained from (Widiatmoro and Nusiaputra 2020) and are only available from 2012 to early 2018. Therefore, production data from 2019 to early 2025 were reconstructed using an exponential decline rate of 2.04% per year, based on the same study. Meanwhile, the enthalpy data were taken from (Horta 2022) and are available only from 2013 to 2020. The final result of the history matching is presented in Figure 11.

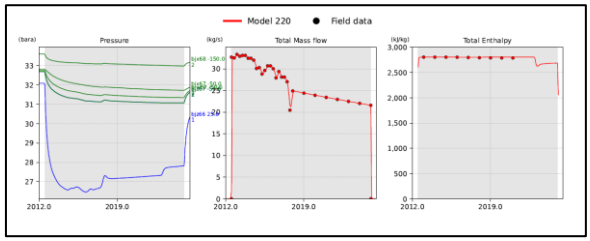

Figure 11. ULB-02 History Matching Result. Indicating that both enthalpy and mass flow have been successfully matched between the model and measured data

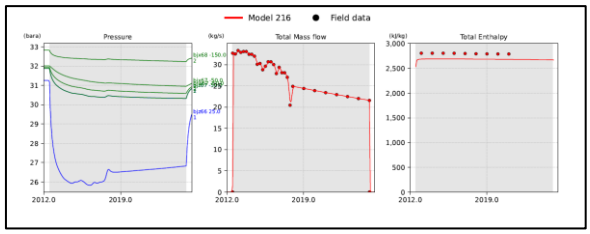

Figure 12. ULB-02 History Matching Result. Showing a good match in mass flow, but an underestimation of enthalpy in the model

To achieve the satisfactory match shown in Figure 11, both porosity and the relative permeability curves were adjusted during the calibration process. Initially, the model underestimated enthalpy compared to the measured data, as illustrated in Figure 12. Porosity values were reduced from the default value of 0.1, ranging from 0.03 in the basement to 0.25 near the surface. Lowering the porosity contributed to enhanced boiling during pressure decline, thereby increasing steam generation. In conjunction with this, the relative permeability curve was modified to allow steam to flow more easily at lower water saturations, reflecting the water-wet nature of the system. The combination of these adjustments improved the ability of the model to reproduce the observed enthalpy, resulting in a closer match with the field measurements.

2.4 Updated Conceptual Model of Ulumbu Geothermal Field

Following the development of the geological, structural, and alteration models, these components were integrated into the numerically calibrated model and subsequently used to update the Ulumbu Geothermal Field conceptual model, as shown in Figure 13. The revised conceptual model highlights key elements of the geothermal system, including the

location of the reservoir, recharge zones, the caprock that inhibits fluid migration, and fault structures that function as permeability boundaries and conduits for fluid flow. The lithological distribution encompassing the heat source, reservoir, caprock, and surface formations closely resembles the previous conceptual model proposed by (Widiatmoro and Nusiaputra 2020), as shown in Figure 14. Structurally, the northeastern caldera is interpreted as a boundary due to the absence of surface manifestations, while the nearby northeastern fault is identified as a major upflow pathway. Conversely, the southwestern fault is characterised as an outflow pathway. A key novelty of the revised conceptual model is the representation of the steam zone, which originates from beneath the basement and rises vertically through the northeastern conduit fault before spreading laterally beneath the clay cap, characterising the Ulumbu field as a vapor-dominated geothermal system. Reservoir temperatures, as derived from the numerical model, range from 200°C to 250°C, consistent with geothermometry results and well temperature data. Recharge is inferred to occur from both the northern and southern margins of the model, where pyroclastic lithologies dominate and exhibit no alteration process that would reduce permeability.

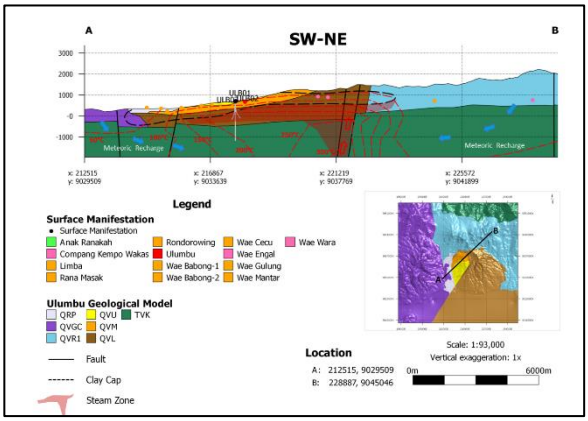

Figure 13: 3D Digital conceptual model (combined 3D model) of Ulumbu Geothermal system

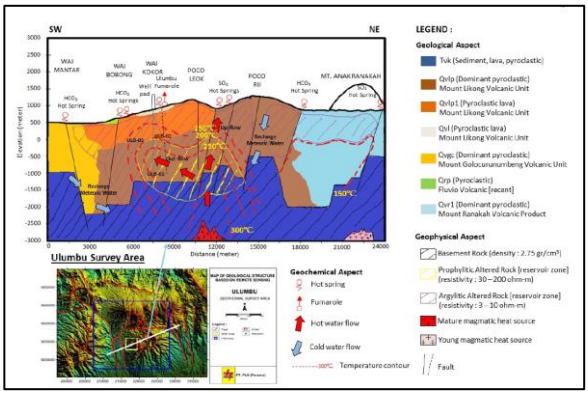

Figure 14. Conceptual Model of Ulumbu Geothermal Field. (Modified from Widiatmoro and Nusiaputra 2020)

3. GROUNDWATER ANALYSIS

Once the enthalpy and mass flow had been successfully matched during the history matching process, the analysis proceeded to evaluate the impact of production from well ULB-02, covering the period from 2012 to 2025, on the water table level, with a specific focus on the plantation areas surrounding the Ulumbu Power Plant.

The initial step involved identifying the block names in the numerical model that correspond to areas where local communities have reported agricultural impacts, allegedly caused by geothermal production. These claims originated from three villages: Wewo, where the geothermal wells are located**,** as well as Lunggar and Mocok, which are situated further from the field. Figure 39 presents the plantation areas identified using Google Earth, which were subsequently imported into Leapfrog and overlaid with the numerical model to determine the relevant block names. Figure 40 shows a plantation map with an area that corresponds to all of the blocks in the numerical model with a rectangular shape. The list of blocks associated with the reported groundwater issues is shown in Table 3.

Figure 15. Distribution of Plantation Areas Surrounding the Ulumbu Geothermal Field, Mapped Using Google Earth Pro

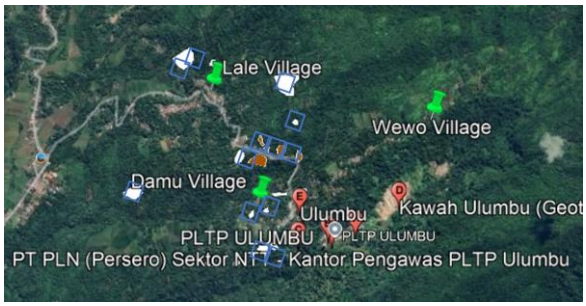

Figure 16. Plantation Map with the block selection related to the plantation area, showing a rectangular shape

ISSN 2703-4275

Table 3: List of the blocks that are associated with the plantation area

No	Village	Block Name	Coordinate		
			X	Y	Z
1	WEWO	bei47	216882.22	9034095.86	570
2	WEWO	bel46	216548.67	9034316.64	590
3	WEWO	bej43	217102.99	9034429.42	650
4	WEWO	bek43	216769.44	9034650.19	650
5	WEWO	bjl40	217323.77	9034762.97	710
6	WEWO	bjo40	216990.22	9034983.74	710
7	WEWO	bjn36	217210.99	9035317.30	790
8	WEWO	bqm33	217431.76	9035650.85	850
9	WEWO	bjb39	216877.44	9035538.07	730
10	WEWO	bpx38	217098.21	9035871.63	750
11	WEWO	bjd44	216323.11	9035425.29	630
12	WEWO	bjc42	216543.88	9035758.85	670
13	WEWO	bed49	215881.56	9034758.19	530
14	LUNGGAR	cle27	221645.62	9036219.54	970
15	LUNGGAR	cld31	221979.18	9035998.76	890
16	MOCOK	cmb18	223980.50	9034674.11	1150
17	MOCOK	cmc24	223646.95	9034894.89	1030

3. RESULT AND DISCUSSION

Pressure changes in each block were calculated from the commencement of production in 2012 through to the most recent production data available in 2025. In addition to analysing pressure variations in the plantation areas, pressure changes were also assessed in associated subsurface zones: the water table, clay cap, gas zone, and liquid zone, to further evaluate the potential influence of production on groundwater conditions. The analysis revealed that in all 17 blocks associated with plantation areas listed in Table 3, the pressure change was effectively zero. However, in the water table blocks within these areas, specifically where gas saturation is zero, the highest observed pressure drop was 0.00046 bar, corresponding to a minimal 4.6 mm decrease in hydraulic head. Deeper zones showed greater pressure declines: the clay cap zone exhibited a maximum pressure drop of 0.22 bar, while the gas and liquid zones experienced pressure reductions of up to 1.351 bar and 1.8 bar, respectively. The pressure change for each block is summarised in Figure 17.

These results suggest that the effect of geothermal production on the water table within the plantation areas is negligible. In contrast, significant pressure changes in the deeper reservoir zones can be directly attributed to geothermal production. Furthermore, the presence of a steam zone capped by a highly impermeable layer serves to hydraulically isolate the reservoir from the shallow aquifer, reinforcing the conclusion that production does not influence the water table in the plantation areas.

It is important to note that this analysis is based on production data that has been successfully calibrated against field measurements. However, the potential influence of non-production factors, such as water usage during drilling, site preparation, and land modification, on groundwater levels was not included in this study and warrants further investigation.

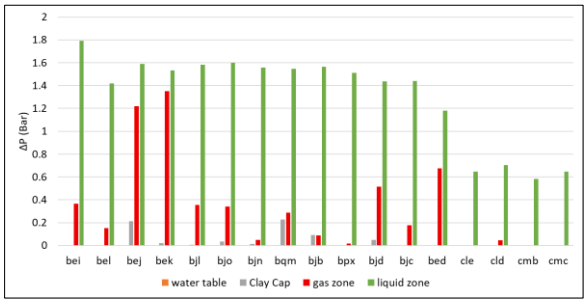

Figure 17: Pressure Change of Each Block Classified based on Zone

4. CONCLUSION

This study has successfully assessed the impact of geothermal production at the Ulumbu Geothermal Field on changes in the local water table, providing insight into potential effects on the surrounding agricultural sector. The results were obtained through the development of a 3D calibrated numerical model, constructed using limited publicly available data from published papers and theses, and further strengthened by an uncertainty quantification process involving an ensemble of acceptable model realisations. This approach enhances the reliability of the water table impact analysis.

A natural-state calibrated model was developed using a hot plate as the heat source, as pressure and temperature data indicated the presence of vapor in the wells. The simulation results show steam rising from the base of the model and flowing vertically through an NE–SW fault conduit, then spreading laterally within the reservoir (L) formation, confirming that Ulumbu is a vapor-dominated system. This interpretation is supported by the production history matching, which achieved a good alignment between the steady-state model and measured production data. The model maintained relatively constant enthalpy values between 2803 and 2787 kJ/kg from June 2012 to January 2025, indicating dry steam production.

The calibrated model was then used to evaluate water table variations, which remained within negligible thresholds during production and posed no significant risk to agricultural systems. However, this analysis has a limited scope, focusing only on the production impacts from 2012 to 2025. It does not account for non-production factors or the influence of climate change, such as variations in rainfall intensity, which could also affect groundwater levels.

The methodology developed in this study provides a solid technical framework for evaluating water table dynamics in the context of geothermal development, an issue of growing importance. While the current findings indicate that geothermal production has minimal impact on the water table, further research is recommended to explore a broader range of development scenarios, particularly under varying extraction rates. This framework can also be used to assess the impact of geothermal exploration on the New Zealand cases, especially in Rotorua, which has a shallow system to the surface manifestation that acts as a tourism sector.

ACKNOWLEDGMENT

My deepest thanks go to the *Lembaga Pengelola Dana Pendidikan (LPDP)* Scholarship for providing the financial support that enabled me to pursue the Master of Energy program so that I can conduct this research. I am also grateful to Seequent for providing a Leapfrog software license, which was invaluable for my research.

REFERENCES

EBTKE, Ditjen. 2016. *Potensi Panas Bumi Indonesia*. Jilid 2.

Grant, Malcolm A., and Paul F. Bixley. 2011. "Concepts of Geothermal Systems." In *Geothermal Reservoir Engineering*, , 9–28.

Hilah, Alfani Restu, and Ir. Henk Subekti, Dipl. Eng., M.E. 2022. "Analisa Penurunan Laju Produksi Pada Sumur X Pltp Ulumbu." *Prosiding Seminar Nasional Teknologi Energi dan Mineral* 2(1): 11–18.

Horta, Angela B. 2022. "PERENCANAAN SKENARIO PENGEMBANGAN LAPANGAN PANAS BUMI ULUMBU DITINJAU DARI ASPEK KEEKONOMIAN."

Kurniawan, Iqbal, S. Sutopo, Heru Berian Pratama, and Reza Adiprana. 2019. "A Natural State Model and Resource Assessment of Ulumbu Geothermal Field." *IOP Conference Series: Earth and Environmental Science* 254(1).

Nugraha, Rony P, John O'sullivan, Michael J O'sullivan, and Fathan H Abdurachman. 2022. "Geothermal Modelling: Industry Standard Practices." *Proceedings, 47th Workshop on Geothermal Reservoir Engineering*: 1–12.

O'Sullivan, John et al. 2023. "An Integrated, Mesh-Independent Geothermal Modelling Framework." *Environmental Modelling and Software* 163(July 2022): 105666.

O'Sullivan, M. J., and J. P. O'Sullivan. 2016. Geothermal Power Generation: Developments and Innovation *Reservoir Modeling and Simulation for Geothermal Resource Characterization and Evaluation*. Elsevier Ltd.

Pruess, Karsten, Curt Oldenburg, and George Moridis. 1999. "TOUGH2 User's Guide, Version2.0." (November).

Sulasdi, Didi. 1996. "Exploration of Ulumbu Geothermal Field, Flores-East Nusa Tenggara, Indonesia." *PROCEEDINGS, 21st Workshop on Geothermal Engineering, Standford University, Standford, California*: 51–54.

Teredi, Ernest L, Agustinus Sukarno, and Marselinus Joni Jaya. 2022. "Derita Rakyat Dan Lingkungan Di Balik PLTP Ulumbu." : 1–32.

Widiatmoro, Tony, and Yodha Y Nusiaputra. 2020. "Production Decline and Reservoir Pressure Decline Evaluation on the Ulumbu Geothermal Field, Flores, East Nusa Tenggara, Indonesia." *Proceedings World Geothermal Congress 2020+1 Reykjavik, Iceland, April - October 2021* (October): 1–10.

Yuono, R. T., and Y. Daud. 2020. "Reservoir Simulation of Ulumbu Geothermal Field Using TOUGH2 and ITOUGH2 Simulator." *IOP Conference Series: Earth and Environmental Science* 538(1).